Presentation, analysis, and simulation of active alignment strategies for the James Webb Space Telescope

Robert S. Upton

Space Telescope Science Institute,
3700 San Martin Drive,
Baltimore, MD,
USA 21218

ABSTRACT

This paper presents three characteristics in the simulated active alignment strategy of the James Webb Space Telescope. The first includes the analysis and comparison of a baseline active alignment strategy with a damped least squares strategy. This baseline utilizes prior knowledge by means of direct human operator interaction to engage sets of telescope compensators to target specific aberration signatures. The baseline is compared to a damped least-squares strategy that utilizes simultaneous engagement of all telescope compensators without explicit human operator interaction to achieve a least-squares telescope compensation. Second, we discuss how the active alignment of the JWST is encapsulated in a linear optical model developed at the Space Telescope Science Institute. This linear optical model provides a framework for an efficient and robust description of the optical control properties of the JWST and clearly articulates the necessity for having a multi-instrument multi-field wavefront sensing strategy to overcome control system non independence and the effects of non-common path errors in the main wavefront sensing camera. Finally, we present analytical results that explicitly map the telescope wavefront responses to the telescope control modes, and we present Monte-Carlo optical performance simulation results that demonstrate the efficacy of the damped least-squares active alignment and the prior-knowledge active alignment schemes.

Keywords: Optical control modeling, segmented aperture telescopes, inverse problems

1. INTRODUCTION

The James Webb Space Telescope (JWST) is a space-based infrared optimized optical system with a 6.5 m primary mirror and a total of three powered mirrors.[1] The powered mirrors deliver near infrared (NIR) light with wavelength range $0.6\mu m < \lambda < 5\mu m$ and mid infrared (MIR) light with wavelength range $5\mu m < \lambda < 15\mu m$ to a suite of four scientific instruments.[1] The scientific field-of-view for JWST is approximately 20 arc-min by 10 arc-min, with the field footprint of the five instruments[2] shown in Fig. 1.

The JWST will be delivered in a folded state to its orbital location at the second Lagrange point associated with the Moon, Earth, and Sun. Once JWST is delivered the telescope will be unfolded, its primary mirror segments phased, and the secondary mirror positioned to give a least-squares aligned state of the telescope. The process of aligning the telescope for scientific observations occurs over a duration of 5-6 months and utilizes a number of different wavefront sensing strategies that target specific compensating degrees-of-freedom (DOFs) of the primary mirror segments and secondary mirror. For example, the relative piston orientations of the primary mirror segments are determined by means of a fringe sensing technique that is similar to the fringe phasing system utilized by the Keck telescopes,[3] and the smaller scale pistons of the segments, in-plane DOF orientations, and segment radii-of-curvatures are determined by means of a hybrid diversity phase retrieval algorithm.[4]

In this paper, two wavefront commissioning processes are presented and compared. The first process, a version of the JWST baseline, utilizes targeted wavefront sensing and compensation strategies to achieve a least-squares aligned state of the telescope. The targeted correction of specific aberrations by specific DOFs defines a prior-knowledge use of wavefront sensing and control. The second process uses a damped least-squares
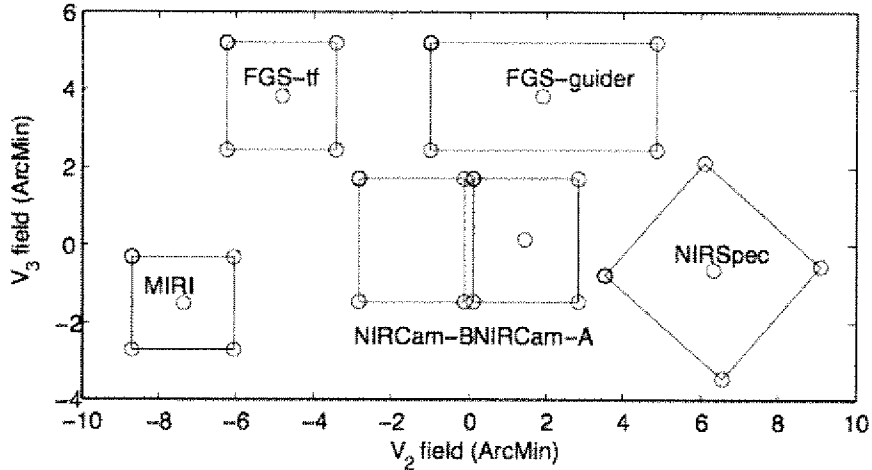
Figure 1. A plot of the footprints of the suite of five instruments on the JWST scientific field-of-view. The axes $V2$ and $V3$ denote the horizontal and vertical field positions on the instrumentation focal plane in a right-handed co-ordinate system. The 29 field points shown in the Figure correspond to the field points utilized in the multi-instrument multi-field wavefront sensing and control strategy.

reconstructor that introduces Tikhonov filtering. Tikhonov filtering[5-7] is a numerical conditioning formalism that can be used to dampen the smallest singular values in a positive semi-definite non-square matrix.[8,9] The damped-least squares wavefront control strategy is not proposed as viable alternative to the baseline. However, useful insights are gained into the optical control properties of the JWST and the simulated baseline wavefront commissioning process by presentation and comparison of the damped least-squares approach.

The Space Telescope Science Institute (STScI) has developed an optical control modeling capability in order to engage the optical control simulation and modeling verification analysis discussion within the JWST community. Simulation and modeling of wavefront commissioning plans, and wavefront control strategies are an essential component of the STScI role in the JWST mission.

This paper presents: A simulated version of the JWST baseline wavefront commissioning process (Section 2); The optical control models developed at the Space Telescope Science Institute (STScI) that are used to simulate the baseline and damped least-squares wavefront commissioning processes (Section 3); The optical control properties of the JWST (Section 4); The results of Monte-Carlo simulations of the wavefront commissioning processes (Section 5). The models utilized in the simulation of optical control and wavefront sensing make use of linearized vector mappings between telescope compensating DOFs and wavefront errors measured in the telescope exit pupil. The integration of phase retrieval wavefront sensing techniques into the STScI optical control models is ongoing.

A simulated version of the multiple-instrument multiple-field (MIMF) wavefront sensing strategy, used in the JWST baseline wavefront control, is presented in this discussion. MIMF is used to overcome the non-full rank nature of the telescope control laws that result from non-indpdendence of the telescope compensating DOF and the effects of non-common path error in the main wavefront sensing camera.

2. WAVEFRONT COMMISSIONING PROCESS

The wavefront commissioning process starts with the JWST in its post-launch state with the pre-deployment of the secondary mirror and folded state of the primary mirror. After approximately 180 days the residual uncorrectable OTE RMS wavefront error over the entire JWST scientific field is not to exceed the residual callout from the wavefront sensing and control error budget. After wavefront commissioning, the telescope is in its aligned and scientifically operational state. Table 1 contains the steps taken during the version of the baseline

wavefront commissioning process encapsulated in the Webb SLOM optical model. Table 1 describes each step, and the regions of the scientific field utilized for wavefront sensing for each step. Steps 4, 5, and 6 are expected to happen iteratively, depending on the effects of the main wavefront sensing camera non-common path errors and the effect of the non-common path error on the residual focal plane tilts introduced by the secondary mirror during step 5 of the simulated baseline wavefront commissioning process. The main wavefront sensing camera is the shortwave channel of the Near Infrared Camera scientific instrument (NIRCam A).[2] Much of the discussion in this paper pertains to steps 4, 5, and 6 of the baseline wavefront commissioning process. That is, the JWST primary and secondary mirror fine-phasing and MIMF steps.

Table 1. The baseline wavefront commissioning plan encapsulated in the Webb SLOM optical model. The first column indicates the control step and corresponding location in the scientific field used to extract the wavefront error signal, the second column describes the degree-of-freedom (DOF) correction. After the MIMF control step, the primary mirror is fine phased once more.

Control step and wavefront signal	DOF correction
1. Secondary mirror sweep	Not modeled
2. Global alignment	Clocking and decenters
3. Image stacking NIRCam A central field	Tilts
4. Primary mirror fine phasing NIRCam A central point	1.Tilts 2.Segment z piston 3.Radius of curvature 4.Clocking
5. Secondary mirror fine phasing Five NIRCam A field points	Five secondary mirror RB DOFs
6. MIMF 29 field points over scientific field	The secondary mirror optimized for least-square alignment over the OTE field

The simulated baseline wavefront commissioning plan utilizes a cascaded optical control and compensation scheme during steps 4, 5, and 6 to achieve a least-norm aligned state of the telescope. The cascaded compensation approach modeled in Webb SLOM utilizes groupings of primary mirror segment compensators with similar sensitivities to achieve least-squares correction. For example, during the baseline wavefront commissioning process the tilts and the pistoning of the primary mirror segments are used as the first compensating group for correction. Once these out-of-plane DOFs have been utilized, the radius-of-curvature of each segment is engaged whilst the out-of-plane DOFs are forced to maintain their corrected states. Then the in-plane clocking of the segments are engaged. Finally, the in-plane decenters of the segments are engaged, whilst the remaining DOFs are forced to maintain their corrected states. Hence, the cascaded approach utilizes DOFs that have a significant degree of linear independence between them simultaneously. That is, the interaction matrices utilized in each primary mirror correction step are well conditioned. Once the set of cascaded primary mirror correction steps are engaged during step 4, the secondary mirror is engaged in step 5. Then the secondary mirror is engaged once again during step 6. After secondary mirror engagement in step 6 the primary mirror is phased by implementing step 4 once again.

The damped least-squares alignment strategy presented in this discussion combines all the primary mirror DOFs into simultaneous compensation motions that result in a least-norm aligned state of the primary mirror. The primary mirror correction is followed by rigid body alignment of the secondary mirror. This process is repeated between one and five times. The number of iterations chosen is based on empirical analysis. Simulta-

neous engagement of all primary mirror compensating DOFs requires a multiple-field wavefront sensing scheme to overcome the tilt and decenter ambiguity associated with each primary mirror segment. Hence, the damped least-squares alignment strategy utilizes the five NIRCam A field points shown in Fig. 1

3. OPTICAL CONTROL MODEL

The optical control models utilized in this analysis are developed and are maintained by the Space Telescope Science Institute (STScI). The models are collectively designated the name Webb SLOM* . Webb SLOM is among other optical control simulation tools that have been developed by the JWST optical modeling community.[10,11] STScI has developed an optical control modeling capability to engage in the optical control simulation and modeling verification analysis and discussion within the JWST community. Simulation of optical control strategy and wavefront commissioning plans is an essential component of the STScI role in the JWST mission.

Webb SLOM is contained in the MATLAB and ZEMAX modeling environments in a client-server active *dynamic data exchange* (DDE) relationship.[12] The control laws are contained in primary mirror and secondary mirror Jacobian interaction matrices that map the motions of the JWST compensating DOFs to the linearized wavefront responses calculated at the JWST exit pupil. The wavefront responses are decomposed into radial and azimuthal polynomial functions that are orthonormal over the hexagonal pupil aperture.[13,14] It should be noted that the model does not include any phase retrieval wavefront sensing algorithms at this time. In this analysis the wavefront error signal is assumed to be formed in a perfect and noiseless way. The Jacobian interaction matrices and their inverses are contained within MATLAB. The JWST model contained in ZEMAX includes a fully segmented primary mirror as a set of non-sequential raytrace objects. Figure 2 contains a schematic indicating the logical flow of information and data utilized in obtaining the optical control interaction matrices and the Monte-Carlo performance analysis of the JWST optical control. The interaction matrix in Fig. 2 is designated the symbol H. Figure 2 also contains a screen capture of the Webb SLOM GUI front end that is used to simulate the JWST baseline wavefront commissioning process. Figure 3 contains a ZEMAX rendering of the JWST optical model utilized by Webb SLOM.

3.1 Derivation of the optical control law for Webb SLOM

The fundamental relation[9,15] describing the mapping process from one vector space containing $\mathbf{f}$ to a conjugate vector space containing $\mathbf{g}$ by an operator represented by $\mathbf{h(g|f)}$ is,

$$\mathbf{g} = \int_\Sigma \mathbf{h(g|f)f df}. \tag{1}$$

In this discussion $\mathbf{f}$ represents a subset of JWST DOFs and $\mathbf{g}$ the wavefront errors. The wavefront errors in $\mathbf{g}$ are coefficients of radial and azimuthal polynomials that are orthonormal over a hexagonal aperture. For primary mirror control the hexagonal apertures are the individual primary mirror segments. For secondary mirror control the hexagonal aperture is the best-fitting hexagon over the entire OTE exit pupil. The operator $h(\mathbf{g|f})$ represents the optical control system. The operator $h(\mathbf{g|f})$ is linearized to form a Jacobian matrix H, which consists of matrix elements $h_{i,j}$. Hence the optical control system encapsulated by Eq. (1) may be represented by the linear system,

$$g_i = h_{0,i} + \sum_j h_{ij} f_j. \tag{2}$$

The Jacobian matrix consists of columns that each contain the wavefront error response to input DOFs. The elements $h_{i,j}$ are generated from a least-squares linear fit of wavefront response data to three different input magnitudes of DOF variations. The extent to which the columns contained in the matrix H are linearly independent is directly representative of the linear independence of the telescope DOFs for a particular wavefront sensing geometry in the telescope field-of-view.

The JWST compensating DOFs are tilts, clocking, decenters of the primary mirror segments, and the local radius-of-curvature variations of the primary mirror segments, and the secondary mirror rigid body DOFs. The

---

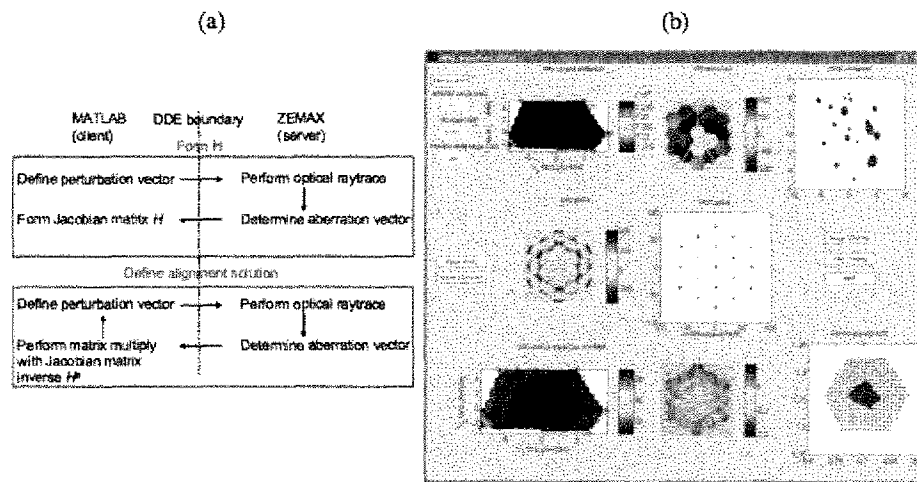*Webb SLOM is extracted from the terms James Webb Space Telescope Space Telescope Science Institute Linear Optical Model

(a)

MATLAB   DDE boundary   ZEMAX
(client)   (server)
             Form H

Define perturbation vector ——→ Perform optical raytrace

Form Jacobian matrix H ←—— Determine aberration vector

Define alignment solution

Define perturbation vector ——→ Perform optical raytrace

Perform matrix multiply ←—— Determine aberration vector
with Jacobian matrix
inverse H⁻¹

(b)

Figure 2. **(a)** A schematic showing the flow of data and information between the ZEMAX and MATLAB components of Webb SLOM. MATLAB controls the instances of ZEMAX by DDE. The schematic represents the formation of an interaction matrix and the Monte-Carlo simulation of the JWST misalignment. **(b)** The Webb SLOM GUI used to simulate the JWST baseline wavefront commissioning plan. The combination of the DDE interface between MATLAB and ZEMAX combined with the flexibility to generate MATLAB GUI's provides opportunity for powerful and widespread use of the model.
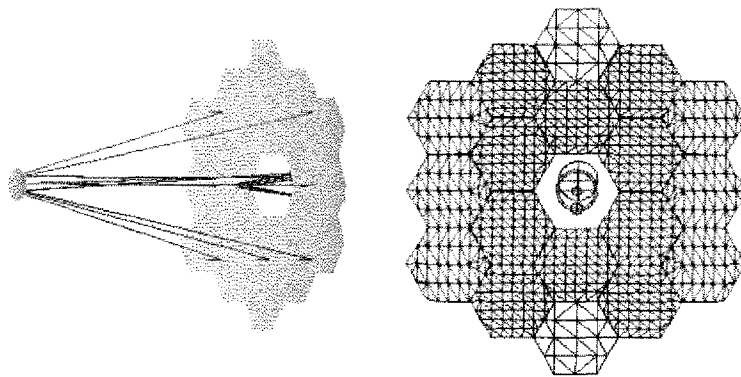

Figure 3. An oblique view 3D solid rendering and a 3D face-on layout view of the JWST optical model represented in ZEMAX. The JWST optical model is controlled by code contained within MATLAB that interfaces with ZEMAX by DDE.

secondary mirror is located remotely from any pupil within the telescope. Hence, different science field points have different footprints over the secondary mirror. As a result any errors in the shape of the secondary mirror phase surface and in distinguishing between secondary mirror tilts and decenters requires wavefront responses from multiple field points. In addition, if simultaneous optical control of the tilts and decenters of the primary mirror segments is required, multiple field point wavefront responses have to be utilized to form an adequate least-squares aligned state of the primary mirror.

The fundamental requirement for multiple field points arises from overcoming the non-independence of tilting and decentering conical surfaces. However, in the case of the primary mirror, the sequential, or cascaded, control of the most to least sensitive DOFs can overcome the multiple field requirement for primary mirror control. The simulated JWST baseline wavefront commissioning plan during the primary mirror fine phasing allows the most sensitive out-of-plane primary mirror segment tilts and pistons to be adjusted first, whilst maintaining the in-plane motions and radii-of-curvature of the segments. Then, the radii of curvatures of the primary mirror segments are changed whilst the remaining DOFs are maintained; Then the mirror segment tilts and pistons and radii of curvatures are maintained, whilst the in plane decenters, and clockings are adjusted. This "strong-weak-strong" optical control strategy† utilizes the full rank nature of truncated optical control matrices and contains columns that are wavefront error responses to subsets of the telescope controllable DOFs. This point is described in more detail in Subsection 4.3.

3.2 Derivation of the least-squares aligned state generated by the optical control law

The linear system in Eq. (2) in the presence of white Gaussian additive noise can be rewritten as,

$$\mathbf{g} = \mathbf{h_0} + H\mathbf{f} + \mathbf{n}. \tag{3}$$

The Cramer-Rao lower bound[16, 17] is applied to the linear system, subject to the noise process $\mathbf{n}$ to determine the minimum-variance unbiased estimate of Eq. (3). The probability law governing $\mathbf{n}$ is,

$$P(\mathbf{n}) = \frac{1}{(2\pi)^{N/2}\sigma} exp\left[-\frac{1}{2\sigma^2}\mathbf{n}^T\mathbf{n}\right]. \tag{4}$$

The necessary steps to form the Cramer-Rao Lower bound[16, 17] are followed to form the minimum-variance unbiased estimate $\hat{\mathbf{f}}$,

$$\hat{\mathbf{f}} = \left(H^T H\right)^{-1} H^T \left[\mathbf{g} - \mathbf{h_0} - \mathbf{n}\right]. \tag{5}$$

Equation (5) assumes that the matrix H is full rank and is not susceptible to the scalar noise parameter σ. If H is not full rank, it is singular, and the minimum-variance unbiased estimate does not exist. Then the least-norm estimate is utilized. In Webb SLOM the least-norm pseudo-inverse used is the damped reconstructor that utilizes Tikhonov filtering.[5] The least-norm estimate of $\mathbf{f}$ calculated by the damped reconstructor, which in this discussion is assigned the generic term "the damped least-squares reconstructor" is,

$$\hat{\mathbf{f}} = \left[H^T H + \rho I\right]^{-1} H^T \left[\mathbf{g} - \mathbf{h_0} - \mathbf{n}\right]. \tag{6}$$

The most significant results to extract from this Section are the least-squares inverse in Eq. (5) used for the full rank matrix H and the damped-least squares inverse in Eq. (6), which can be used for non-full rank matrices and in the presence of significant noise that may decrease the effective rank of H.

The truncation of H to include only DOF that have similar sensitivities is utilized in the baseline JWST wavefront commissioning process to overcome the poor conditioning of H for primary mirror control. The optical control properties of the baseline wavefront control strategy are presented in Section 4.

---

†This utilization of strong-weak-strong DOFs to perform optical control was communicated to the author by J. Howard and Kong Ha of NASA Goddard Space Flight Center.

4. OPTICAL CONTROL PROPERTIES OF JWST

The linear optical model for the JWST, contains optical control matrices for the primary and secondary mirrors, which are H_{PRIM} and H_{SEC}, respectively. The optical control properties of the JWST are contained in H_{PRIM} and H_{SEC}. As stated the extent to which the columns of the matrices H_{PRIM} and H_{SEC} are linearly independent is the degree of linear independence between the telescope DOFs. The degree-of-linear independence between the telescope DOFs determines the conditioning of the matrix and determines the dimension of its column space. The dimensionality of the telescope column space, and the degree of the telescope linear independence can be quantified by the singular value decomposition (SVD).[12, 19]

The SVD of the control matrix H yields three matrices V, Σ, and U. The matrix V consists of columns that are orthonormal vectors $\mathbf{v}_1, ..., \mathbf{v}_m$ spanning the vector space defined by the wavefront sensing response of the telescope system. These are the left singular vectors. The matrix Σ is a nominally diagonal matrix consisting of μ_n the singular values of the matrix H. The matrix U consists of columns that are orthonormal vectors $\mathbf{u}_1, ..., \mathbf{u}_n$ spanning the telescope DOFs space. These are the right singular vectors. The SVD is written as,

$$H = \sum_{n=1}^{R} \mathbf{v}_n \mathbf{u}_n^T \mu_n. \tag{7}$$

The value R in Eq. (7) is the rank of the matrix. If H were a positive definite square matrix then the vectors $\mathbf{v}_1, ..., \mathbf{v}_n$ and $\mathbf{u}_1, ..., \mathbf{u}_n$ would be the right singular vectors and would be eigenvectors of H and Σ would be a matrix of eigenvalues.

The right singular vectors (span DOF space), and the singular values define the optical control properties of the telescope. The left singular vectors (span wavefront sensing space) and singular values define the wavefront sensing properties of the telescope. In the following subsections the properties of optical control utilizing the damped least squares reconstructor for wavefront commissioning, and the baseline optical control strategy for wavefront commissioning are presented. An essential component to the optical control discussion is the use of the numerically rigorous technique for optical systems sensitivity analysis presented by Chapman.[19]

4.1 Optical control and wavefront sensing modes

The DOF $\mathbf{f}$ and wavefront sensing modes $\mathbf{g}$ can be expressed as the expansions,

$$\mathbf{f} = \sum_{n} (\mathbf{u}_n^T \mathbf{f}) \mathbf{u}_n, \tag{8}$$

$$\mathbf{g} = \sum_{n} (\mathbf{v}_n^T \mathbf{g}) \mathbf{v}_n. \tag{9}$$

Therefore, each of the optical control modes contained in $\mathbf{u}_1, ..., \mathbf{u}_n$ consist of vector components that are equal to the telescope DOFs $\mathbf{f}$. Also, the wavefront sensing modes contained in $\mathbf{v}_1, ..., \mathbf{v}_n$ consist of vector components that are equal to the wavefront sensing vectors $\mathbf{g}$.

The vector space spanning property for $\mathbf{f}$ and $\mathbf{g}$ contained in Eqs. (8) and (9) is utilized in a singular mode based sensitivity analysis technique[19] to determine the greatest telescope DOF contributors to each telescope singular value. The vector space spanning property can also be used in wavefront sensing space to determine the aberration components that contribute most to each singular value. This technique is utilized in a discussion of the optical control properties and wavefront sensing geometry of the Advanced Technology Solar Telescope.[12]

The plots in Figure 4 show the truncated singular values and labeling indicating the primary and secondary mirror DOFs that have the greatest contributions to each truncated singular value. The truncated singular values have almost the same values as the singular values. The truncated singular values are calculated iteratively from a subset of the interaction matrix where the column corresponding to the least sensitive DOF for a particular iteration of the calculation is truncated. The number of iterations in the calculation is equal to the number of singular values minus one. The singular values presented are extracted from a generic 18 segment primary mirror telescope design that contains the same general properties as the JWST.
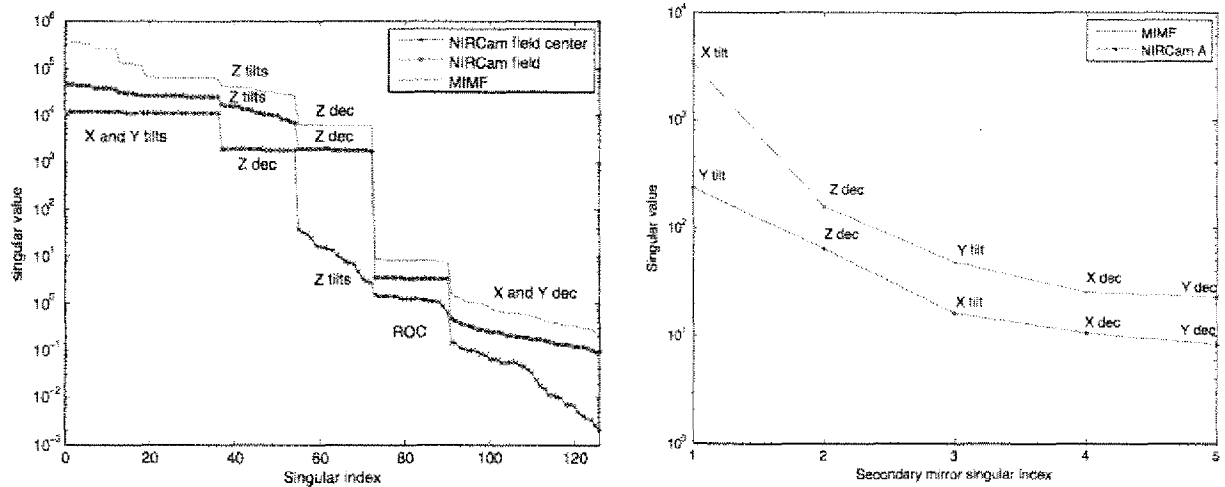
Figure 4. Plots of the truncated singular values corresponding to (left) three different primary mirror optical interaction matrices corresponding to three different wavefront sensing geometries in the field-of-view, and (right) two different secondary mirror optical interaction matrices corresponding to two different wavefront sensing geometries in the field-of-view. The DOFs contributing most to each singular value is indicated in the plot.

The primary mirror singular values plotted in Fig. 4 are calculated for interaction matrices containing a single field point at the NIRCam A field center, five points over the NIRCam A field, and the 29 points shown in Fig. 1. The secondary mirror singular values plotted in Fig. 4 are calculated for interaction matrices containing five points over the NIRCam A field, and the 29 points shown in Fig. 1. The condition numbers for each matrix are similar because the DOFs that are collected in each matrix have similar sensitivities. However, the relative sensitivities between the groups of primary mirror DOFs differ. For example, the relative sensitivities of the the segment pistons along the z axis (z dec) are greater than the clocking (z tilts) for the matrix formed with a single NIRCam A field point. Whereas the sensitivities of the clocking (z tilts) and pistons (z decenters) are switched for the matrices that have more then one field point included in the calculation. The reason for the re-ordering of sensitivities arises from the field dependent aberration signature resulting from clocking (z tilts) compared with the field independent change in focus arising from the z piston.

Optical control of the secondary mirror in Webb SLOM utilizes simultaneous engagement of all the secondary mirror rigid body DOFs to achieve compensation. The simultaneous engagement of all secondary mirror DOFs requires wavefront sensing from more than one field point to overcome the tilt-decenter ambiguity of the secondary mirror.

Table 2. The condition numbers corresponding to the primary mirror interaction matrices that contain all the primary mirror DOFs, the XY tilts (out-of-plane tilts) and pistons (Z decenter), the clocking (Z tilts), XY decenters (in plane decenters), and radius-of-curvatures. All matrices are calculated with respect to the wavefront error response at the center of the NIRCam A field-of-view.

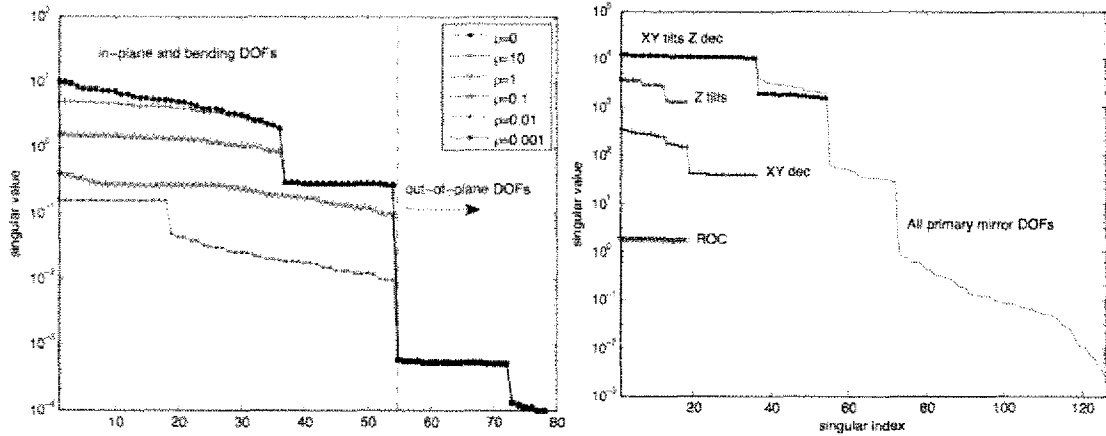| Matrix type	Condition number
All primary mirror DOFs	$5.99e + 06$
XY tilts, piston	8.12
Clocking	3.05
XY decenters	9.01
Radius of curvature	1.09

Figure 5. Plots of the singular values corresponding to: (left) the primary mirror DLS reconstructor with the different damping factors ρ shown, including the case where no damping is introduced. The plot contains a label showing the breakdown between the less sensitive in plane primary mirror segment DOFs, and the more sensitive out-of-plane primary mirror DOFs; and (right) the primary mirror control matrix containing all its DOF, and the singular values corresponding to the control matrices with the DOFs indicated. The matrices are calculated with respect to wavefront error responses at the center of the NIRCam A field-of-view.

4.2 Damped least-squares optical control

For damped least-squares (DLS) optical control during the wavefront commissioning simulations of the JWST primary mirror, the wavefront error signals from the five NIRCam A field points shown in Fig. 1 and the corresponding interaction matrix are used. First the alignment signal for the secondary mirror is calculated, after which the alignment signals for the primary mirror segments are calculated from the residual wavefront error.

The DLS reconstructor introduces the parameter ρ, as shown in Eq. (6), to dampen the effects of the smallest singular values, which become the dominant singular values in the inverse. These smallest singular values, if left undampened, can force the telescope into pathological alignment states, by allowing the most insensitive DOFs to have large values, and to be highly susceptible to noise in the system. The value of ρ to use in the inverse is chosen by trial and error. In the Webb SLOM Monte-Carlo simulations of the primary mirror phasing by the DLS wavefront commissioning, the values chosen for ρ for five correction iterations are 10, 1, 0.1, 0.01, and 0.001, respectively. Each value of ρ is introduced for a different iteration of the reconstructor. There is no damping introduced for the secondary mirror.

Figure 5 in the left pane contains plots of the singular values of the primary mirror DLS reconstructor for six different damping factors. The singular values presented are extracted from a generic 18 segment primary mirror telescope design that contains the same general properties as the JWST. The effect of the damping is to diminish the effect of the less sensitive in-plane primary mirror DOFs. For example, the effect of greater damping values in the first two iterations of the DLS reconstructor is to force the more sensitive out-of-plane DOFs to provide most of the correction. Then after most of the wavefront error has been compensated with the more sensitive out-of-plane DOFs, the residual errors can be corrected by the less sensitive in-plane DOFs. This effect is utilized explicitly in the baseline optical control strategy.

4.3 Baseline optical control

The simulated baseline optical control of JWST utilizes the cascaded optical compensation scheme described in Section 2 to phase the primary mirror and the wavefront error signals from multiple field points to align the secondary mirror. The primary mirror control utilizes the wavefront error signals from a single field point located at the center of the NIRCam A field. In order to overcome the tilt, decenter, and radius of curvature ambiguities associated with primary mirror control at a single field point the baseline primary mirror phasing introduces a

sequence of corrections starting with the more sensitive out-of-plane DOFs, and then the less sensitive radius-of-curvature DOF and in-plane mirror decenters. This process is repeated in an iterative "strong-weak-strong" compensation strategy.

Figure 5 in the right pane contains the singular values of the interaction matrices that contain the out-of-plane tilts, z pistons (z-dec), in clocking (z-tilts), decenters, and radii of curvature (ROC). Table 2 contains the condition numbers for the full primary mirror interaction matrix, and the matrices corresponding to the groups of DOFs utilized in the primary mirror compensation component of the baseline wavefront commissioning plan. The condition numbers presented are extracted from a generic 18 segment primary mirror telescope design that contains the same general properties as the JWST. The condition number for the primary mirror matrix containing all the DOFs spans six orders of magnitudes. This large condition number indicates significant non-independence between the columns of the matrix, which occurs as a result of the tilt and decenter ambiguity of the segments for single field point wavefront sensing. However the condition numbers corresponding to the matrices containing the wavefront responses for the grouped sets of DOFs are not greater than an order of magnitude. Hence, there is significant linear independence between the columns of the matrices containing the grouped DOFs, which is utilized in the "strong-weak-strong" optical control of the primary mirror.

5. MONTE-CARLO SIMULATION RESULTS

Monte-Carlo optical performance simulations are performed under the conditions of scientific instrument non-common path error. The non-common path error in the NIRCam A optical channel is simulated as second-order field dependent astigmatism. The non-common path error in the remaining optical channels are simulated as field independent astigmatism. The field dependent NIRCam A aberration model is the most dominant non-common path error effect. Most of the simulated baseline wavefront commissioning plan utilizes wavefront error signals from the NIRCam A field points shown in the plot contained in Fig. 1. The multi-instrument multi-field (MIMF) wavefront sensing and control strategy utilizes all the field points shown in Fig. 1. MIMF is necessary to sense any residual tilts, or other residual low-order field dependencies in the scientific focal plane that occur as a result of NIRCam A non-common path errors. There is less residual wavefront error over the scientific field-of-view after MIMF, compared with after fine phasing.

A perturbation vector containing random orientations of all the rigid body JWST DOFs and random perturbations to the primary mirror segments radii-of-curvature are introduced into the ZEMAX optical model that is contained in Webb SLOM. The perturbation vector includes the rigid body perturbations to the tertiary mirror. The JWST compensating DOFs include the primary mirror rigid body DOFs and radii-of-curvatures, and the rigid body orientations of the secondary mirror. Figure 6 contains the RMS wavefront errors: resulting from the perturbed optical models; after the DLS and baseline wavefront commissioning of the JWST in the presence of scientific instrument non-common path errors. The RMS wavefront errors resulting from the Monte-Carlo performance analyses are extracted from a generic 18 segment primary mirror telescope design that contains the same general properties as the JWST. The Monte-Carlo simulation results show that the simulated baseline wavefront commissioning plan results in substantially better optical performance than the damped least-squares approach. The improvement in optical performance is greatest along the V_3 instrument axis. In addition the use of MIMF results in a further improvement of optical performance in NIRSpec, FGS-tf, and FGS-guider regions of the scientific fields. Hence, the use of prior knowledge, and a non-damped reconstructor that does not filter any of the control modes during compensation results in optimum optical performance over a wide range of optical deformations to a JWST-like optical system.
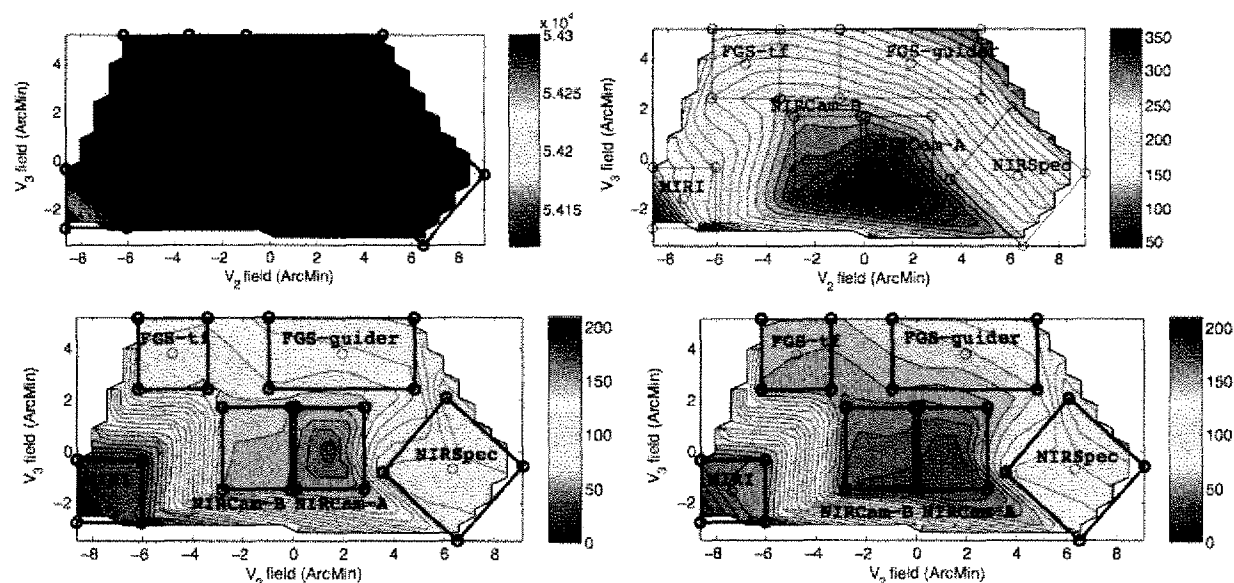
Figure 6. Contour plots of the RMS wavefront errors resulting from (top-left) perturbation of JWST ; (top-right) the DLS correction of JWST; (bottom-left) correction of the JWST alignment up to and including the fine phasing of the primary and secondary mirror; and (bottom-right) correction of the JWST alignment up to and including MIMF. The wavefront sensor signals include non-common path errors from all the scientific instruments.

REFERENCES

[1] Gardner, J. P., Mather, J. C., and etal, "The science requirements of the James Webb Space Telescope," in [Optical, infrared, and millimeter space telescopes], Mather, J. C., ed., Proc. SPIE **5487**, 5487564 (2004).

[2] Davila, P., Bos, B., and etal, "The James Webb Space Telescope science instrument suite: An overview of optical designs," in [Optical, infrared, and millimeter space telescopes], Mather, J. C., ed., Proc. SPIE **5487**, 5487611 (2004).

[3] Chanan, G., Troy, M., and Sirko, E., "Phase discontinuity sensing: A method for phasing segmented mirror in the infrared," Appl. Opt. **38**, 704–713 (1999).

[4] Dean, B. H., Aronstein, D. L., Smith, J. S., and Shiri, R., "Phase retrieval algorithm for JWST flight and testbed telescope," in [Space Telescopes and Instrumentation I], Mather, J. C., ed., Proc. SPIE **6265**, 626511 (2006).

[5] Vogel, C. R., [Computational Methods for Inverse Problems], Society for Industrial and Applied Mathematics (2002).

[6] Paxman, R. G., Barrett, H. H., Smith, W. E., and Milster, T. D., "Image reconstruction from coded data: II Code design," JOSA A **2**, 501–509 (1985).

[7] Maeda, J. and Murata, K., "Restoration of band-limited images by iterative regularized pseudoinverse method," JOSA A **1**, 28–34 (1984).

[8] Strang, G., [Linear algebra and its applications], Brooks/Cole (1988).

[9] Barrett, H. H. and Myers, K. J., [Foundations of Image Science], Wiley (2004).

[10] Howard, J. M., "Optical modeling activities for the James Webb Space Telescope (JWST) project: I. the linear optical model," in [Optical performance modeling], Kahan, M., ed., Proc. SPIE **5178**, 517882 (2004).

[11] Contos, A. R., Acton, D. S., Barto, A., and etal., "Verification of the James Webb Space Telescope (JWST) wavefront sensing and control system," in [JWST: OTE verification], Jacobus Oschmann Jr., Mattheus W. M. McGraauw, H. A. M., ed., Proc. SPIE **7010**, 70100S (2008).

[12] Upton, R. S., "Optical control of the Advanced Technology Solar Telescope," Appl. Opt. **45**, 5881–5896 (2006).

[13] Mahajan, V. N. and ming Dai, G., "Orthonormal polynomials for hexagonal pupils," *Optics Letters* **31**, 2462–2464 (2006).

[14] Upton, R. S. and Ellerbroek, B., "Gram-Schmidt orthogonalization of the Zernike polynomials on apertures of arbitrary shape," *Optics Letters* **29**, 2840–2842 (2004).

[15] Born, M. and Wolf, E., [*Principles of optics: Electromagnetic theory of propagation, interference and diffraction*], Cambridge University Press, sixth ed. (1999).

[16] Kay, S. M., [*Fundamentals of Statistical Image Processing:Estimation Theory Vol. 1*], Prentice Hall (1993).

[17] Frieden, B. R., [*Probability, statistical optics, and data testing*], Springer (1991).

[18] Andrews, H. C. and Hunt, B. R., [*Digital image restoration*], Prentice Hall (1977).

[19] Chapman, H. N. and Sweeney, D. W., "Rigorous method for compensation selection and alignment of microlithographic optical systems," in [*EUV Lithography III*], Vladimirsky, Y., ed., *Proc. SPIE* **3331**, 102 (1998).